

Constraints from LIGO/Virgo and NICER on quark star equation of state

ANG LI,¹ JIN-LIANG JIANG,^{2,3} SHAO-PENG TANG,^{2,3} ZHI-QIANG MIAO,¹ EN-PING ZHOU,⁴ AND REN-XIN XU^{5,6}

¹*Department of Astronomy, Xiamen University, Xiamen, Fujian 361005, China; liang@xmu.edu.cn*

²*Key Laboratory of Dark Matter and Space Astronomy, Purple Mountain Observatory, Chinese Academy of Sciences, Nanjing 210023, China*

³*School of Astronomy and Space Science, University of Science and Technology of China, Hefei, Anhui 230026, China*

⁴*Max Planck Institute for Gravitational Physics (Albert Einstein Institute), Am Mühlenberg 1, Potsdam-Golm, 14476, Germany*

⁵*School of Physics, Peking University, Beijing 100871, China*

⁶*Kavli Institute for Astronomy and Astrophysics, Peking University, Beijing 100871, China*

(Dated: September 29, 2020)

ABSTRACT

We investigate the quark star equation of state within the Bayesian statistical approach using the widely-used bag model, assuming the strange quark matter is in the color-flavor locked phase. Three types of filters are employed for the posterior distribution: Normal atomic nuclei should not decay into nonstrange quark matter, bulk strange quark matter should be more stable than the most bound atomic nuclei, and the lower limit on the maximum mass M_{TOV} . The likelihood functions incorporate observational constraints from the tidal deformability measurement of the GW170817 binary merger by LIGO/Virgo and the measurements of PSR J0030+0451's mass and radius by NICER. The 90% posterior credible boundary around the most probable values of the quark star maximum mass is found to be $M_{\text{TOV}} = 2.15^{+0.16}_{-0.12} M_{\odot}$, with the radius and tidal deformability of a canonical $1.4M_{\odot}$ star being $R_{1.4} = 11.52^{+0.51}_{-0.46}$ km and $\Lambda_{1.4} = 670^{+230}_{-160}$, respectively. Nevertheless, the color superconductivity gap is poorly constrained by those observed global star properties, and no clear evidence about the sound speed behavior in strange quark matter is manifested. A possible probe of the quark pairing gap through future tidal deformability measurement of massive quark stars (close to M_{TOV}) is also discussed.

1. INTRODUCTION

The recently observed GW170817 binary neutron star merger event (Abbott et al. 2017, 2018) has greatly promoted the study of the equation of state (EOS) of dense stellar matter, restricting its stiffness or the degree of freedom of dense matter in the density regime achieved inside compact stars (possibly up to $\approx 8-10 n_0$, with $n_0 = 0.16 \text{ fm}^{-3}$ being the nuclear saturation density) (e.g., Li et al. 2020). Although it is known that the degree of freedom is hadron around nuclear saturation density and the color-flavor locked (CFL) state is the ground state of three-flavor quark matter at asymptotic densities, the phase state of cold QCD matter for intermediate densities ($\sim 1 - 10 n_0$) are unfortunately unknown. A great deal of effort is undergoing in the communities of astrophysics, nuclear physics, and particle physics due to its crucial importance. One key point is still not clear: Does the matter go through a phase transition from hadron matter to quark matter at some intermediate densities, or quark matter is the absolute ground state of strongly interacting matter for interme-

mediate densities? (the conjecture of Bodmer-Witten; Bodmer 1971; Witten 1984). In the latter case, quark stars, self-bound by strong interaction, serve as a new class of pulsar-like objects, which are fundamentally different from the gravity-bound neutron stars.

It has been proposed that binary quark star scenario could be consistent with the observation of GW170817 and its electromagnetic counterparts (e.g., Bauswein et al. 2009; Paulucci et al. 2017; Zhou et al. 2018; Lai et al. 2020). Moreover, a magnetar with quark star EOS is preferred as the post-merger remnant to explain some groups of short gamma-ray burst observations (e.g., Li et al. 2016, 2017). Therefore it is interesting and useful to learn what constraints we can obtain on quark star models from multimessenger observations for better understanding the nature of pulsar-like objects.

Previously, we have shown in Zhou et al. (2018) that the tidal deformability measurement of the GW170817 merger event by LIGO/Virgo has allowed to substantially restrict the parameter space of quark star EOS if combining with the mass constraints of the massive pul-

sars whose masses are precisely measured. The purpose of this work is to reexamine our previous constraints, where only the boundaries of the mass and tidal deformability observations were used, to incorporate the prior knowledge of those observations into our analysis using a Bayesian inference approach. In particular, the heaviest pulsar to date (MSP J0740+6620) has been newly detected whose mass is reported with 68.3% credibility interval, $M = 2.14^{+0.10}_{-0.09} M_{\odot}$ (Cromartie et al. 2020). We further include a simultaneous estimation of the mass and radius of PSR J0030+0451 by the NASA *Neutron Star Interior Composition ExploreR (NICER)* mission (Riley et al. 2019; Miller et al. 2019; Raaijmakers et al. 2019).

The paper is organized as follows. Section 2 is a brief overview of the Massachusetts Institute of Technology (MIT) bag model adopted for quark star EOS; Section 3 presents the employed observations and the Bayesian analysis for the EOS; In Sec. 4, we discuss the quark star properties, especially the maximum mass M_{TOV} and the radius and the tidal deformability of a canonical $1.4 M_{\odot}$ star, along with the adiabatic index and sound speed in quark matter. We then summarize the paper in Sec. 5. Section 6 contains the Appendix.

2. THE MIT BAG MODEL FOR QUARK STAR EQUATION OF STATE

In an earlier paper, we (Zhou et al. 2018) performed the calculations on the mass-radius and tidal deformability for quark stars using MIT bag model EOSs (Alcock et al. 1986; Haensel et al. 1986), in which we have also considered the finite mass of strange quark, QCD corrections due to gluon-mediated interactions between quarks [characterized by the parameter a_4 (~ 0.7 ; Fraga et al. 2001; Alford et al. 2005; Bhattacharyya et al. 2016; Li et al. 2017)] as well as the pairing of quarks. It was shown that finite strange quark mass and a_4 parameter had weak influences on the results, and the stiffness of the EOS is mainly determined by the effective bag constant B_{eff} . For normal unpaired quark stars, $B_{\text{eff}}^{1/4}$ is found to be in the range of [134.1, 141.4] MeV, to be consistent with tidal deformability measurement of GW170817 (Abbott et al. 2017) and the two-solar-mass pulsar observation (Antoniadis et al. 2013). It was also found that considering the color superconductivity (as also mentioned in the review of Baiotti 2019) could loose the tension between a large maximum mass ($\sim 2.14 M_{\odot}$; Cromartie et al. 2020) and a low tidal deformability ($\Lambda_{1.4} = 190^{+390}_{-120}$; Abbott et al. 2018).

In the present study, we again use the EOSs based on the MIT bag model and consider that quark stars constitute charge-neutral bulk strange quark matter in

Table 1. Most probable intervals of the bag model parameters (90% confidence level) constrained by the joint analysis for the two priors: Uniform (U) and logarithmic uniform (LogU) distributions.

Parameters	Prior type	Constraint	Joint analysis
$B_{\text{eff}}^{1/4}/\text{MeV}$	U(125, 150)	$135.26^{+11.90}_{-8.74}$	$140.88^{+7.72}_{-6.26}$
	LogU(125, 150)	$131.39^{+9.03}_{-5.76}$	$136.75^{+4.13}_{-4.49}$
a_4	U(0.4, 1)	$0.55^{+0.18}_{-0.12}$	$0.63^{+0.15}_{-0.15}$
	LogU(0.4, 1)	$0.57^{+0.16}_{-0.11}$	$0.68^{+0.13}_{-0.12}$
Δ/MeV	U(0, 100)	$38.29^{+45.98}_{-34.20}$	$46.43^{+40.76}_{-40.78}$
	LogU(0.1, 100)	$2.91^{+50.89}_{-2.77}$	$1.70^{+26.66}_{-1.57}$

the CFL state. Since the symmetry enforces the equal number of flavors, there are no electrons in the CFL phase. The grand canonical potential per unit volume of quark matter is written as:

$$\Omega = \sum_{i=u, d, s} \Omega_i^0 + \frac{3\mu^4}{4\pi^2}(1 - a_4) - \frac{3\Delta^2\mu^2}{\pi^2} + B_{\text{eff}}, \quad (1)$$

with $\mu = (\mu_u + \mu_d + \mu_s)/3$ the average chemical potential. Ω_i^0 is the grand canonical potential for particle type i described as ideal Fermi gas. We may neglect the quark masses of the up and down quarks and choose the strange quark mass $m_s = 100$ MeV. The third term denotes the pairing energy associated with color superconductivity, with Δ being the CFL pairing gap. Δ can be as high as 100 MeV but is very uncertain.

Using the basic thermodynamic relations, the energy density e and pressure p of the system are obtained with

$$e = \Omega + \sum_i \mu_i n_i, \quad (2)$$

$$p = n \frac{\partial}{\partial n} \left(\frac{e}{n} \right), \quad (3)$$

where $n = (n_u + n_d + n_s)/3$ is the baryon number density.

Integrating the Tolman-Oppenheimer-Volkoff (TOV) equations, one gets the star's mass and the radius for each central density. The tidal Love numbers k_2 is obtained from the ratio of the induced quadrupole moment Q_{ij} to the applied tidal field E_{ij} (Damour & Nagar 2009; Damour et al. 1992; Hinderer 2008, 2009; Postnikov et al. 2010): $Q_{ij} = -k_2 \frac{2R^5}{3G} E_{ij}$. The dimensionless tidal deformability Λ is related to the compactness M/R and the Love number k_2 through $\Lambda = \frac{2}{3} k_2 (M/R)^{-5}$. Since the stars' global properties (M, R, Λ) have one-to-one correspondence with the underlying EOS, they are therefore characterized by three independent parameters ($B_{\text{eff}}, a_4, \Delta$).

3. OBSERVATIONS, CONSTRAINTS, AND BAYESIAN ANALYSIS

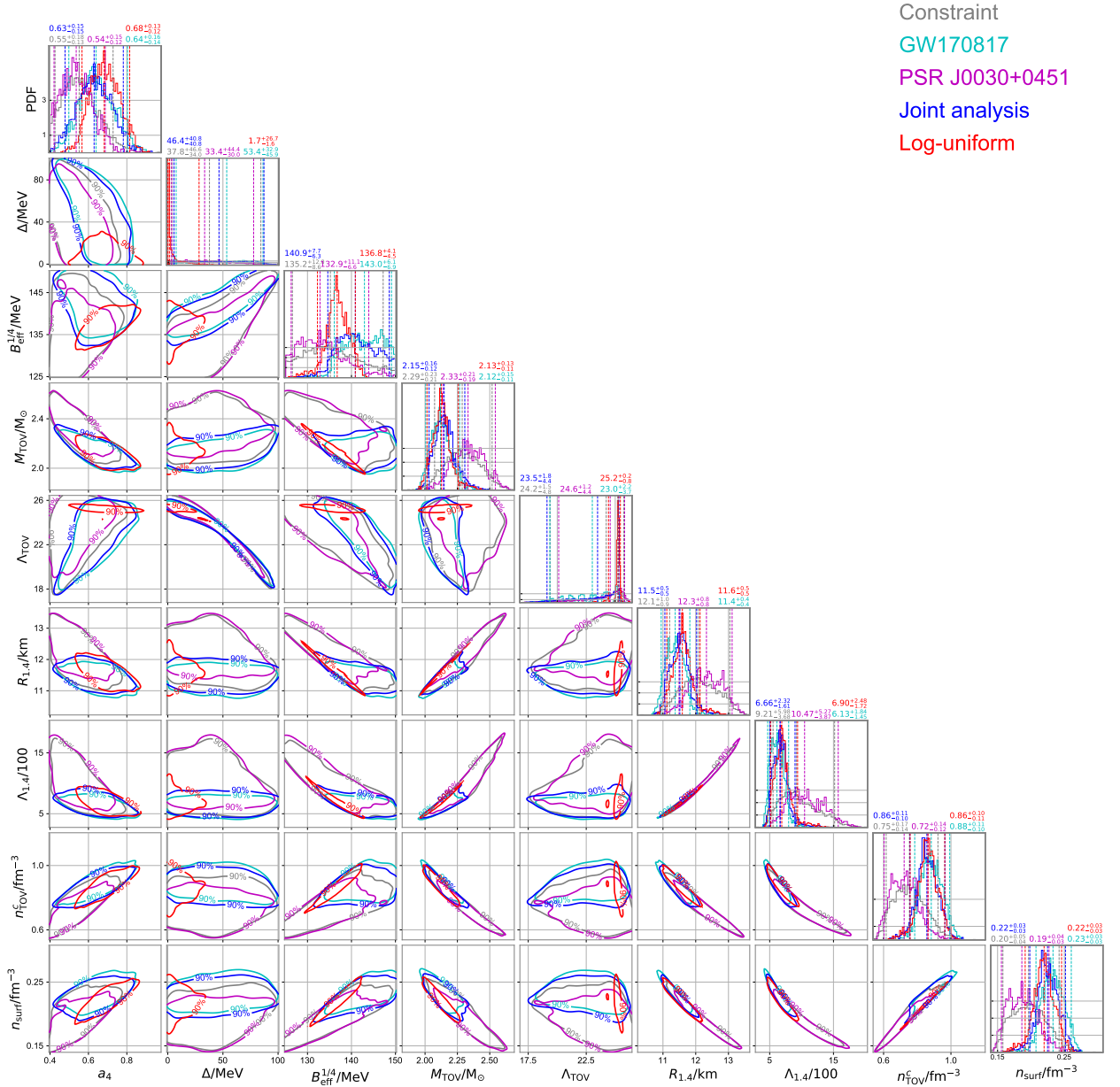


Figure 1. Posteriors distributions of the MIT bag model parameters ($B_{\text{eff}}^{1/4}$, a_4 , Δ) and quark star properties (M_{TOV} , Λ_{TOV} , $R_{1.4}$, $\Lambda_{1.4}$, n_{TOV}^c , n_{surf}), together with those of the employed constraints (the stability conditions plus the M_{TOV} soft-cut). The contours are the 90% credible regions for the parameters. The grey, cyan, magenta, and blue contours represent the results conditioned on the uniform prior for the constraint test, the GW170817 test, the PSR J0030+0451 test, and the joint analysis test, respectively (see Sec. 4 for details). The joint analysis for the log-uniform prior is also shown in red contours for comparison.

3.1. Bayesian analysis

The well-known binary merger event GW170817 caught by LIGO/Virgo detectors (Abbott et al. 2017) has provided us a great opportunity to constrain the parameters of EOS that described by the theoretically motivated parameterizations. Assuming that the noise in the LIGO/Virgo detectors is Gaussian and stationary, the likelihood of a gravitational event used to perform Bayesian inference is often expressed as

$$L(d|\vec{\theta}_{\text{GW}}) \propto \text{Exp}\left(-2 \int \frac{|d(f) - h(\vec{\theta}_{\text{GW}}, f)|^2}{S_n(f)} df\right), \quad (4)$$

where $S_n(f)$, $d(f)$, and $h(\vec{\theta}_{\text{GW}}, f)$ respectively denote the power spectral density (PSD), the frequency domain data, and the frequency domain waveform generated using parameter set $\vec{\theta}_{\text{GW}}$. The tidal deformability Λ encoded in the gravitational wave strain data can be mapped from the mass through the dense matter EOS. Thus the EOS parameters together with component masses can be incorporated to construct the gravitational wave parameters $\vec{\theta}_{\text{GW}}$ (see, e.g., Tang et al. 2020; Jiang et al. 2020). Here we take the publicly available strain data¹ and PSDs² of GW170817 (Abbott et al. 2019), together with the waveform model IMRPHE-NOMD_NRTIDAL (Dietrich et al. 2017) to do the analysis. The observational data of GW190425 (Abbott et al. 2020) is not included in this analysis as scenarios such as black hole-neutron star merger is also viable for GW190425 (Han et al. 2020) and the EOS constraint is not very strong.

Recently, with the dedicated observations of *NICER*, the mass-radius of the PSR J0030+0451 are measured with an unprecedented accuracy (Riley et al. 2019; Miller et al. 2019), which is also informative for constraining the EOS. We thus incorporate the *NICER* measurement results to constrain our quark star model by using a Gaussian Kernel Density Estimation (KDE) of the posterior sample \vec{S} of mass and radius in the best fit ST+PST model (Riley et al. 2019):

$$L(d|\vec{\theta}_{\text{EOS}}, p_c) = \text{KDE}(M, R | \vec{S}), \quad (5)$$

where $\vec{\theta}_{\text{EOS}} = \{B_{\text{eff}}, a_4, \Delta\}$, p_c is the central pressure of PSR J0030+0451, the M and R are respectively the mass and radius calculated by TOV integral using $\{B_{\text{eff}}, a_4, \Delta, p_c\}$. Since the two results of Riley et al. (2019) and Miller et al. (2019) are consistent with each other, we only adopt the best fit scenario of Riley et al.

(2019), which leads to little difference comparing with adopting the measurements in Miller et al. (2019).

By employing the python-based BILBY (Ashton et al. 2019) and PYMULTINEST (Buchner 2016) packages, we simultaneously inference the gravitational wave parameters, M - R observations as well as the MIT bag model parameters that describe the quark matter.

3.2. Priors and constraints

To improve the nest sampling's converging rate, we marginalize the coalescence phase parameter in the likelihood and fix the source's sky location determined by the electromagnetic observations (Abbott et al. 2017; Levan et al. 2017). As for the priors of the other parameters in $\vec{\theta}_{\text{GW}}$, we take a similar choice presented in Tang et al. (2020). For the parameters $\vec{\theta}_{\text{EOS}}$ that construct the EOS of quark star, following Zhou et al. (2018), we assign reasonably wide boundaries to them as $B_{\text{eff}}^{1/4} \in [125, 150] \text{ MeV}$, $\Delta \in [0, 100] \text{ MeV}$, $a_4 \in [0.4, 1]$, with which both uniform and logarithmic uniform distributions are investigated. For technical reasons, the lower bound of the logarithmic uniform distribution can not be zero; Thus, we set a reasonable lower bound 0.1 for Δ in the logarithmic uniform case.

Two stability constraints for quark star EOS are adopted: First, the energy per baryon for non-strange quark matter should satisfy $(E/A)_{\text{ud}} \geq 934 \text{ MeV}$ to guarantee the observed stability of atomic nuclei; Second, $(E/A)_{\text{uds}} \leq 930 \text{ MeV}$ is required, according to the hypothesis that strange quark matter is absolutely stable (Bodmer 1971; Witten 1984). We also take the lower bound on the maximum mass M_{TOV} placed by MSP J0740+6620 (Cromartie et al. 2020). Instead of incorporating the mass measurement of this source by using a 'hard' cutoff, i.e., choosing a value which is larger than the possible 'true' mass of this source (usually the $1-\sigma$ lower bound), we use a 'soft' cutoff by sampling a mass from the mass distribution of J0740+6620 in each MCMC iteration step and reject the EOS parameter that do not support such a mass.

4. RESULTS AND DISCUSSION

We carry out five main tests to investigate how each data set and constraint affect the result, namely: (1) Constraint, where we consider the stability condition and the M_{TOV} constraint described in Sec. 3.2; (2) GW170817, where we consider the constraints in (1) and the gravitational wave data of GW170817; (3) PSR J0030+0451, where we consider the constraints in (1) and the *NICER* measurement of PSR J0030+0451; (4) Joint analysis, where we join the data of PSR J0030+0451 and GW170817 together with the constraints in (1); (5) Log-uniform, same with the test

¹ <https://www.gw-openscience.org/eventapi>

² <https://doi.org/10.7935/KSX7-QQ51>

Table 2. Most probable quark star properties (90% confidence intervals) obtained with the posterior distributions for the two priors. For the log-uniform prior, only the results of the joint analysis is shown. M_{TOV} is the maximum mass, and n_{TOV}^c , R_{TOV} and Λ_{TOV} are the corresponding central density, radius, and tidal deformability, respectively. $R_{1.4}$ and $\Lambda_{1.4}$ are the radius and tidal deformability for a canonical $1.4M_{\odot}$ star, respectively. n_{surf} is the surface density. $c_{s,\text{max}}^2/c^2$ is the maximum squared sound speed scaled by the squared speed of light.

Test/properties	M_{TOV}/M_{\odot}	R_{TOV}/km	Λ_{TOV}	$R_{1.4}/\text{km}$	$\Lambda_{1.4}$	$n_{\text{TOV}}^c/\text{fm}^{-3}$	$n_{\text{surf}}/\text{fm}^{-3}$	$c_{s,\text{max}}^2/c^2$
Constraint	$2.29^{+0.23}_{-0.21}$	$12.49^{+1.31}_{-1.17}$	$24.2^{+1.6}_{-4.8}$	$12.09^{+0.97}_{-0.88}$	920^{+600}_{-370}	$0.75^{+0.17}_{-0.14}$	$0.20^{+0.05}_{-0.04}$	$0.333^{+0.044}_{-0.000}$
GW170817	$2.12^{+0.15}_{-0.11}$	$11.55^{+0.62}_{-0.58}$	$23.0^{+2.2}_{-3.7}$	$11.37^{+0.45}_{-0.43}$	610^{+180}_{-140}	$0.88^{+0.11}_{-0.10}$	$0.23^{+0.03}_{-0.03}$	$0.337^{+0.042}_{-0.004}$
PSR J0030+0451	$2.33^{+0.21}_{-0.19}$	$12.80^{+1.13}_{-1.09}$	$24.6^{+1.2}_{-4.4}$	$12.33^{+0.78}_{-0.84}$	1050^{+530}_{-390}	$0.72^{+0.14}_{-0.12}$	$0.19^{+0.04}_{-0.03}$	$0.333^{+0.034}_{-0.000}$
Joint analysis	$2.15^{+0.16}_{-0.12}$	$11.73^{+0.72}_{-0.61}$	$23.5^{+1.8}_{-4.4}$	$11.52^{+0.51}_{-0.46}$	670^{+230}_{-160}	$0.86^{+0.11}_{-0.10}$	$0.22^{+0.03}_{-0.03}$	$0.333^{+0.048}_{-0.000}$
Log-uniform	$2.13^{+0.13}_{-0.11}$	$11.73^{+0.73}_{-0.61}$	$25.2^{+0.2}_{-0.8}$	$11.59^{+0.54}_{-0.47}$	690^{+250}_{-170}	$0.86^{+0.10}_{-0.11}$	$0.22^{+0.03}_{-0.03}$	$0.333^{+0.000}_{-0.000}$

(4) except that all the EOS parameters are set to Log-uniform (see Table 1).

4.1. Quark star properties revisited in the bag model

The current Bayesian inference directly connects the astrophysical observables with the underlying quark star EOSs. In Figure 1. We report the marginalized posterior probability distribution functions (PDFs) of three bag model EOS parameters ($B_{\text{eff}}^{1/4}$, a_4 , Δ) plus six quark star properties (M_{TOV} , Λ_{TOV} , $R_{1.4}$, $\Lambda_{1.4}$, n_{TOV}^c , n_{surf}) and their correlations. The most probable values of the EOS parameters and their 90% confidence boundaries are summarized in Table 1, and those of various quark star properties are summarized in Table 2.

From Figure 1, we see that two EOS parameters ($B_{\text{eff}}^{1/4}$ and a_4) are relatively well-constrained and the results depend weakly on the prior choice: $B_{\text{eff}}^{1/4} = 140.88^{+7.72}_{-6.26}$ ($136.75^{+4.13}_{-4.49}$) and $a_4 = 0.63^{+0.15}_{-0.15}$ ($0.68^{+0.13}_{-0.12}$) for the uniform prior (the log-uniform prior). It is noted that the inferred a_4 values are close to the value suggested in Fraga et al. (2001).

The strong dependence of both M_{TOV} and $\Lambda_{1.4}$ on B_{eff} was previously recognized and there is a strong linear correlation between M_{TOV} and $\Lambda_{1.4}$ in logarithm scale (Zhou et al. 2018). We see here again the strong positive correlation between M_{TOV} and $\Lambda_{1.4}$ (or $R_{1.4}$), since the M_{TOV} , $\Lambda_{1.4}$, $R_{1.4}$ values all increase with the EOS stiffness. We also find that the $\Lambda_{1.4} - R_{1.4}$ relation can be well fitted by $\Lambda_{1.4} = a_2 R_{1.4}^2 + a_1 R_{1.4} + a_0$, where the best fit gives $a_2 = 9.51 \times 10^1$, $a_1 = -1.79 \times 10^3$, and $a_0 = 8.71 \times 10^3$, with a maximum residual 3.07%. This strong correlation yields a nearly independent translation from a $\Lambda_{1.4}$ measurement to a $R_{1.4}$ constraint, and vice versa.

We address in the following two interesting findings:

- $n_{\text{surf}}/n_{\text{TOV}}^c$ as characteristic of the EOS stiffness: There are strong negative correlation between $M_{\text{TOV}}/\Lambda_{1.4}/R_{1.4}$ and the quark star surface den-

sity n_{surf} as well as the central density n_{TOV}^c of a maximum-mass quark star, suggesting that $n_{\text{surf}}/n_{\text{TOV}}^c$ can be regarded as characteristics of the EOS stiffness. Moreover, the most probable values for these two parameters are $n_{\text{surf}} = 0.22^{+0.03}_{-0.03} \text{ fm}^{-3}$ (slightly higher than n_0) and $n_{\text{TOV}}^c = 0.86^{+0.11}_{-0.10} \text{ fm}^{-3}$ (around $\sim 5n_0$). The results are robust against different priors.

- $\Delta - \Lambda_{\text{TOV}}$ correlation:

It is seen in Figure 1 and Tables 1-2 that both Δ and Λ_{TOV} are not affected much by both the constraints (more details can be found in Appendix 6.1) and the available mass, radius, and tidal deformability data considered here. They are essentially much sensitive to the chosen prior type. Nevertheless, our analyses reveal that Δ and Λ_{TOV} are nicely anti-correlated and can be well fitted by $\Lambda_{\text{TOV}} = b_2 \Delta^2 + b_1 \Delta + b_0$. The best fit gives $b_2 = -7.75 \times 10^{-4}$, $b_1 = -2.33 \times 10^{-3}$, and $b_0 = 2.53 \times 10^1$. Meanwhile, the fractional residual is well described by a Gaussian distribution with zero mean and a standard deviation of 0.88%. We emphasize that although the data considered here may not shed light on the uncertain color superconductivity gap in quark matter, future measurements of more binary merger events, with a component mass close to the maximum mass, hold the promise of constraining the gap parameter significantly.

4.2. EOS, mass-radius relations and tidal deformability

In Figure 2, we report the posterior distributions of the quark star EOS, its mass-radius relation as well as the mass vs. tidal deformability relation. As expected, the data from GW170817 (low tidal deformability) can effectively prevent the pressure (or radius) from being too big while the data from PSR J0030+0451 (a large radius) do the opposite. The $R_{1.4}$ value corresponding

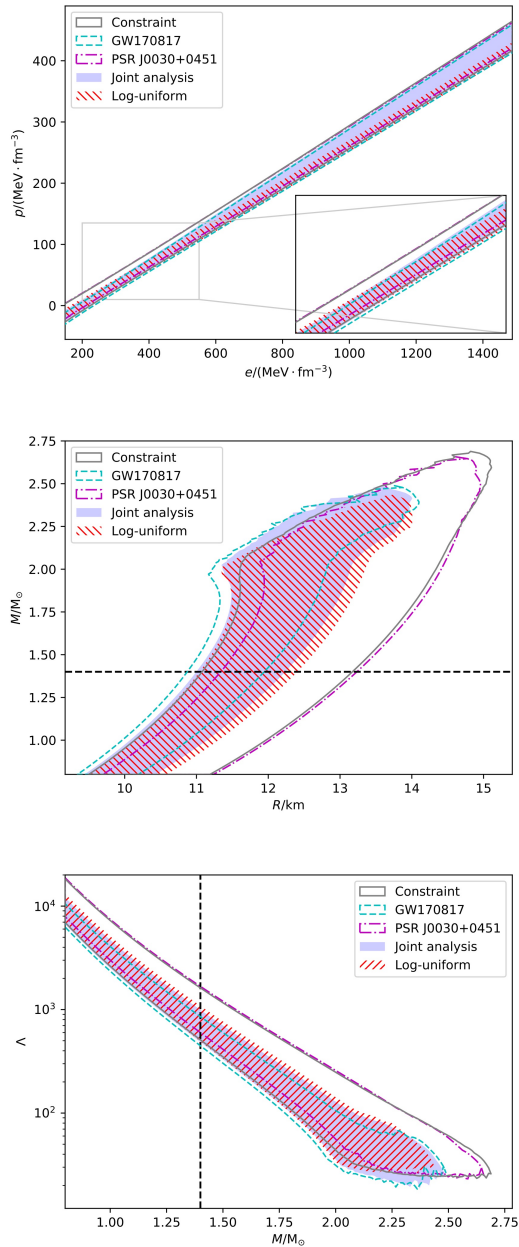


Figure 2. Posterior distributions of the EOS (upper), the mass-radius relation (middle), and the mass versus tidal deformability relation (lower), together with those of the employed constraints (the stability conditions plus the M_{TOV} soft-cut). The grey, cyan, and magenta lines show the connected 95% credible regions conditioned on the uniform prior of the constraint test, the GW170817 test, and the PSR J0030+0451 test, respectively (see Sec. 4 for details). The joint analysis for the uniform prior is shown in the blue-shaded band. The joint analysis for the log-uniform prior is also shown in the red-hatched region for comparison. The horizontal and vertical lines in the middle and lower panels indicate $M = 1.4M_\odot$.

to the data from GW170817 (from PSR J0030+0451) is $11.37^{+0.45}_{-0.43}$ km ($12.33^{+0.78}_{-0.84}$ km). They both contribute to narrowing down the low-density EOS uncertainty band since the related compact objects are low-mass stars with a mass around or lower than $1.4M_\odot$.

The joint analysis for the uniform prior (the log-uniform prior) of $R_{1.4}$ and $\Lambda_{1.4}$ are finally $11.52^{+0.51}_{-0.46}$ km ($11.59^{+0.54}_{-0.47}$ km) and 670^{+230}_{-160} (690^{+250}_{-170}), respectively. Assuming both bodies of GW170817 were neutron stars that are described by the same EOSs, from reproducing the same waveform from LIGO/Virgo and additionally fulfill the two-solar-mass constraint, the $R_{1.4}$ ($\Lambda_{1.4}$) was found to be $11.9^{+1.4}_{-1.4}$ km (190^{+390}_{-120}) (Abbott et al. 2018). Therefore the quark star radius is similar to the neutron star one, but the tidal deformability is larger than that of neutron stars. It can be understood from the fact that quark stars have a much flatter density profile from the surfaces to the centers than neutron stars, while most neutron stars' masses are concentrated at the centers.

The high-density EOS is most sensitive to massive pulsars' mass measurement and has been more or less settled by the constraints. The incorporation of the data from GW170817 significantly lower the maximum mass, for example from $2.29^{+0.23}_{-0.21}M_\odot$ to $2.12^{+0.15}_{-0.11}M_\odot$ in the uniform prior. The resulting quark star maximum mass for the uniform prior is found to be $2.15^{+0.16}_{-0.12}M_\odot$, and similarly $2.13^{+0.13}_{-0.11}M_\odot$ for the log-uniform prior, which are surprisingly comparable with M_{TOV} got by neutron star assumptions (Shao et al. 2020). Using the posterior samples of the joint analysis conditioned on the uniform prior, we also evaluate the radii of MSP J0740+6620 and PSR J1614-2230 to be $12.4^{+1.1}_{-0.4}$ km and $12.2^{+0.7}_{-0.7}$ km, respectively, awaiting to be tested soon by the observation of NICER (Bogdanov et al. 2019).

4.3. Adiabatic index and sound speed

In the upper panel of Figure 3, we report the posterior distributions of the adiabatic index $\Gamma = (e + P)(dP/de)/P$ in strange quark matter. Below ~ 250 MeV/fm^3 , Γ generally shows a sharp decrease with the density, indicating that the quark interactions get weak with density. At high densities, Γ approaches the ultra-relativistic limit of $4/3$ in each case of analysis.

The constant-speed-of-sound parametrization (Alford et al. 2013) has been widely used in the literature for modelling quark matter EOS (see e.g., Miao et al. 2020), making use of the weak density-dependence of the speed of sound ($c_s = \sqrt{dP/de}$). We see in the lower panel of Figure 3 that the squared sound speed c_s^2 (given in the unit of the squared speed of light) is indeed close to the conformal limit of $1/3$ in all density domain, which can be expected from the nearly parallel behavior of the

5. SUMMARY

In this work, we have performed the following investigations: (1) We use the MIT bag model for quark matter EOS where three physical parameters (B_{eff} , a_4 , and Δ) are varied independently; We treat both the stability and the M_{TOV} constraints as prior knowledge of the quark matter EOS ahead of an application of quark stars; A special soft-cut for applying the M_{TOV} constraint is newly introduced; (2) We use a Bayesian inference approach which allows us to explicitly incorporate prior knowledge of the tidal deformability measurement of GW170817 by LIGO/Virgo and the simultaneous estimation of the mass and radius of PSR J0030+0451 by *NICER*; It is thus a more direct and consistent utilization of the observations; (3) We finally provide the posterior probability distributions over the EOS model parameters and the quark star properties; (4) We also examine the dependence of the obtained results on the prior selection for (B_{eff} , a_4 , and Δ).

We contribute updated and stringent parameter ranges for future studies of quark stars within the MIT bag model, especially for B_{eff} and a_4 . The quark star maximum mass M_{TOV} is found to be in the range of $2.03 - 2.31M_{\odot}$, with $R_{1.4}$ and $\Lambda_{1.4}$ in the ranges of $11.06 - 12.03$ km and $510 - 900$, respectively, to the 90% credibility interval. The results should be of great help for identifying the postmerger remnants of GW170817-like events, as well as the central engines of possible accompanying short gamma-ray bursts, in their multi-messenger studies. Furthermore, we newly discover a potential probe for the uncertain Δ parameter through future gravitational-wave signals on massive quark stars' tidal deformability close to their maximum mass. The adiabatic index and sound speed in quark matter are discussed and deserve more study in the future.

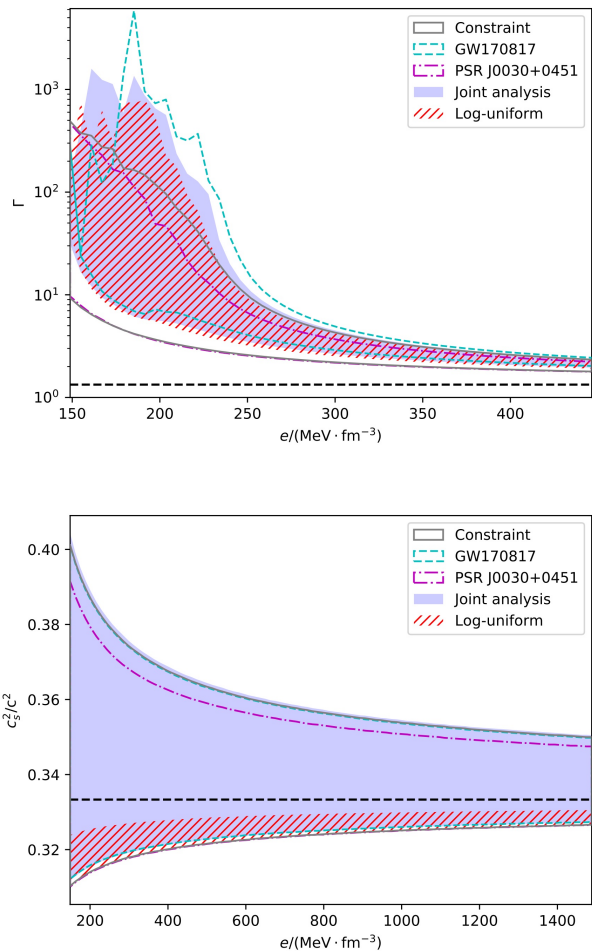


Figure 3. Same with Figure 2, but for the adiabatic index Γ (upper) and squared sound speed c_s^2 (lower; Given in the unit of the squared speed of light) as functions of the energy density e . In the upper and lower panels, the ultra-relativistic limit of $4/3$ and the conformal limit of $1/3$ are shown as the horizontal dashed lines, respectively.

EOSs in Figure 2. Large quark star masses beyond two solar mass is not necessarily resulted from significant enhancements of the sound speed in quark matter, as shown in some model calculations (e.g., Xia et al. 2019). The most probable maximum values of the sound speeds (e.g., in the range of $0.333 - 0.381$ for the uniform prior) and their 90% confidence intervals are also collected in Table 2.

Nevertheless, it is noted that there are appreciably higher probabilities in the uniform prior than in the log-uniform prior for the sound speed to go beyond $1/3$; See more discussions in Appendix 6.2. In the present stage, with only the global properties (M , R , Λ) of the stars available, it is still difficult to conclude whether c_s approaches the $1/3$ limit from below or from above.

ACKNOWLEDGMENTS

We are thankful to Prof. Yizhong Fan and Dr. Zhenyu Zhu for helpful discussions. The work was supported by the National Natural Science Foundation of China (Grant No. 11873040). This research has made use of data and software obtained from the Gravitational Wave Open Science Center <https://www.gw-openscience.org>, a service of LIGO Laboratory, the LIGO Scientific Collaboration and the Virgo Collaboration. LIGO is funded by the U.S. National Science Foundation. Virgo is funded by the French Centre National de Recherche Scientifique (CNRS), the Italian Istituto Nazionale della Fisica Nucleare (INFN) and the Dutch Nikhef, with contributions by Polish and Hungarian institutes.

6. APPENDIX

6.1. *The role of individual constraints*

In this appendix, we report the role played by different constraints introduced in Sec. 3.2. As shown in Figure 4, applying the stability constraint (cyan) together with the M_{TOV} constraint (blue) can effectively limit the parameter spaces of B_{eff} and a_4 , but not Δ . Both parameter spaces of $B_{\text{eff}}^{1/4}$ and a_4 are effectively limited by the stability and the M_{TOV} constraints themselves before applying the GW170817 and PSR J0030+0451 data. Those values of the joint analysis (given in the fourth column of Table 1) by reproducing the mass-radius and tidal deformability observations are slightly larger than those from only the constraints (given in the third column of Table 1). On the other hand, because of the strong correlation among M_{TOV} , $\Lambda_{1.4}$, $R_{1.4}$, n_{surf} , and n_{TOV}^c , the M_{TOV} constraint also influence these global properties. Besides, the stability constraint strongly affect M_{TOV} and $R_{1.4}$, in comparison to the pure uniform prior, it disfavors the high value tail of M_{TOV} and $R_{1.4}$ (see Figure 5).

6.2. *Note on c_s posteriors in the log-uniform prior*

In this appendix, we address the result of the speed of sound obtained in the log-uniform case. We notice that we generally have two kinds of EOSs in our model: the first kind has the maximum sound speed at the zero pressure point, while the sound speed of the second kind reaches its maximum $1/\sqrt{3}$ at asymptotic density. Interestingly, we find that the fraction of the second kind EOS's posterior points is sensitive to the energy gap Δ , which is loosely constrained by the data we considered in this work. Besides, it is found that the lower Δ , the EOSs behave more like the second kind. Since the log-uniform prior leads to much smaller Δ value than the uniform prior, we thus naturally get very different

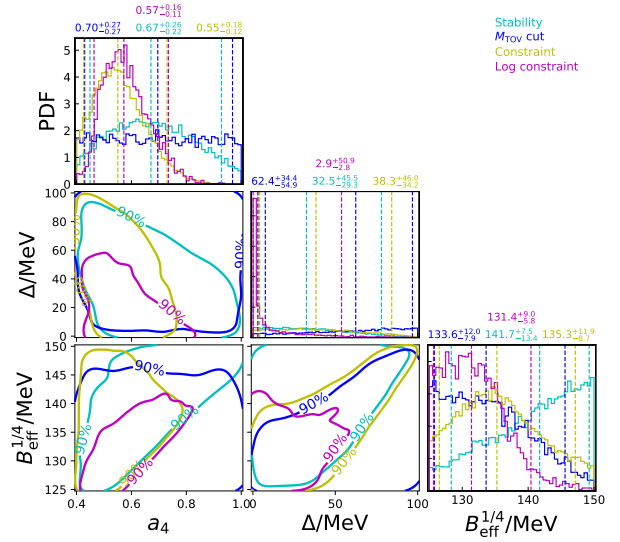


Figure 4. PDFs of three MIT bag model parameters ($B_{\text{eff}}^{1/4}$, a_4 , Δ) to the 90% credibility level. The cyan and blue contours represent the results conditioned on the uniform prior with the stability constraint and the M_{TOV} constraint (see Sec. 3.2 for details), respectively. The results with both the constraints are shown with brown contours, and the corresponding results conditioned on the joint analysis are shown in magenta contours.

density-dependence behavior of the sound speed for the log-uniform prior in comparison to that of the uniform prior (see Figure 3 in the lower panel).

Software: Bilby (Ashton et al. 2019, version 0.5.5, ascl:1901.011, <https://git.ligo.org/lscsoft/bilby/>), PyMultiNest (Buchner 2016, version 2.6, ascl:1606.005, <https://github.com/JohannesBuchner/PyMultiNest>).

REFERENCES

- Abbott, B. P., Abbott, R., Abbott, T. D., et al. 2017, *ApJL*, 848, L12
- Abbott, B. P., Abbott, R., Abbott, T. D., et al. 2020, *ApJL*, 892, L3
- Abbott, B. P., Abbott, R., Abbott, T. D., et al. 2018, *PhRvL*, 121, 161101
- Abbott, B. P., Abbott, R., Abbott, T. D., et al. 2019, *Physical Review X*, 9, 031040
- Abbott, B. P., Abbott, R., Abbott, T. D., et al. 2017, *PhRvL*, 119, 161101
- Alcock, C., Farhi, E., & Olinto, A. 1986, *ApJ*, 310, 261
- Alford, M., Braby, M., Paris, M., et al. 2005, *ApJ*, 629, 969
- Alford, M. G., Han, S., & Prakash, M. 2013, *PhRvD*, 88, 083013
- Antoniadis, J., Freire, P. C. C., Wex, N., et al. 2013, *Science*, 340, 448
- Ashton, G., Hübner, M., Lasky, P. D., et al. 2019, *Astrophysics Source Code Library*
- Ashton, G., Hübner, M., Lasky, P. D., et al. 2019, *ApJS*, 241, 27
- Baiotti, L. 2019, *Progress in Particle and Nuclear Physics*, 109, 103714
- Bauswein, A., Janka, H.-T., Oechslin, R., et al. 2009, *PhRvL*, 103, 011101
- Bhattacharyya, S., Bombaci, I., Logoteta, D., et al. 2016, *MNRAS*, 457, 3101
- Bodmer, A. R. 1971, *PhRvD*, 4, 1601
- Bogdanov, S., Guillot, S., Ray, P. S., et al. 2019, *ApJL*, 887, L25
- Buchner, J. 2016, *Astrophysics Source Code Library*
- Cromartie, H. T., Fonseca, E., Ransom, S. M., et al. 2020, *Nature Astronomy*, 4, 72
- Damour, T., Soffel, M., & Xu, C. 1992, *PhRvD*, 45, 1017
- Damour, T. & Nagar, A. 2009, *PhRvD*, 80, 084035
- Dietrich, T., Bernuzzi, S., & Tichy, W. 2017, *PhRvD*, 96, 121501
- Fraga, E. S., Piasarski, R. D., & Schaffner-Bielich, J. 2001, *PhRvD*, 63, 121702
- Haensel, P., Zdunik, J. L., & Schaefer, R. 1986, *A&A*, 160, 121
- Han, M.-Z., Tang, S.-P., Hu, Y.-M., et al. 2020, *ApJL*, 891, L5
- Hinderer, T. 2009, *ApJ*, 697, 964
- Hinderer, T. 2008, *ApJ*, 677, 1216
- Jiang, J.-L., Tang, S.-P., Wang, Y.-Z., et al. 2020, *ApJ*, 892, 55
- Lai, X. Y., Xia, C. J., Yu, Y. W., et al. 2020, *arXiv:2009.06165*
- Levan, A. J., Lyman, J. D., Tanvir, N. R., et al. 2017, *ApJL*, 848, L28
- Li, A., Zhu, Z.-Y., Zhou, E.-P., et al. 2020, *arXiv:2007.05116*
- Li, A., Zhang, B., Zhang, N.-B., et al. 2016, *PhRvD*, 94, 083010
- Li, A., Zhu, Z.-Y., & Zhou, X. 2017, *ApJ*, 844, 41
- Miao, Z., Li, A., Zhu, Z., et al. 2020, *arXiv:2006.00839*
- Miller, M. C., Lamb, F. K., Dittmann, A. J., et al. 2019, *ApJL*, 887, L24
- Paulucci, L., Horvath, J. E., & Benvenuto, O. 2017, *International Journal of Modern Physics Conference Series*, 45, 1760042
- Postnikov, S., Prakash, M., & Lattimer, J. M. 2010, *PhRvD*, 82, 024016
- Raaijmakers, G., Riley, T. E., Watts, A. L., et al. 2019, *ApJL*, 887, L22
- Riley, T. E., Watts, A. L., Bogdanov, S., et al. 2019, *ApJL*, 887, L21
- Shao, D.-S., Tang, S.-P., Sheng, X., et al. 2020, *PhRvD*, 101, 063029
- Tang, S.-P., Jiang, J.-L., Gao, W.-H., et al. 2020, *ApJ*, 888, 45
- Witten, E. 1984, *PhRvD*, 30, 272
- Xia, C., Zhu, Z., Zhou, X., et al. 2019, *arXiv:1906.00826*
- Zhou, E.-P., Zhou, X., & Li, A. 2018, *PhRvD*, 97, 083015